# Vibration-based monitoring of helicopter epicyclical gears

Victor Girondin, Morel Hervé, Komi Midzodzi Pekpe, Jean Philippe Cassar

# Vibration-based monitoring of helicopter epicyclical gears

**V. Girondin** [1,2], **H. Morel** [1], **K. M. Pekpe** [2], **J. P. Cassar** [2]
[1] EUROCOPTER F-13725 Marignane Cedex, France,
e-mail: **victor.girondin@eurocopter.com**

[2] LAGIS UMR CNRS 8219,
Université Lille 1 Boulevard Langevin 59655 Villeneuve d'Ascq
e-mail: **victor.girondin@ed.univ-lille1.fr**

## Abstract
Epicyclical gears in helicopters are the most sophisticated part of the mechanical transmission monitored, as a result of its numerous sub-components included, its low accessibility for sensor mounting and its complex dynamical behavior. Some analytical and finite element models have suggested to anticipate the vibratory response. However, the external forces that apply to the system during the flight, the complexness of the mechanical design and the multiple power transfer paths, make quite difficult an accurate prediction of the vibratory response received by the accelerometer. Utilizing this prediction for a condition monitoring purpose would lead to poor performances. For this reason, a signal oriented model of vibrations for epicyclical gears is preferred. This model allows for the anticipation of the influence of some damages. Two indicators are proposed to detect the presence of a crack similar to that of a transverse crack on the carrier. These first one uses the cyclic coherence and the second one takes advantage of cyclostationary component separation. The indicators are tested on data recorded from an Eurocopter's testing rig and have permitted to follow the growth of the crack.

## 1 Introduction

Most of the time, the epicyclical gears in helicopters play, the role of final mechanic reduction between the main gearbox (with outputs rotating at $\approx$ 20Hz) and the hub (rotating at $\approx$ 5Hz). Eurocopter's epicyclical gears have fixed ring and carrier attached to the mast, [1]. Planetary gear arrangements permit to satisfy optimal performances on compactness, noise redution and high torque-to-weight ratio. However ,its complex geometry and low accessibility makes it hard to monitor and maintain. Morever, the compactness makes the subelements very sensitive to the other close elements. For example, one damage on one planet bearing can lead to carrier cracks. Some strategies exist to limit damage propogation, for example, the optimization of the reduction ratio in order to maximize the number of cycles necessary for two teeth mounted on the ring and one planet to meet again in a row. Moreover the planets are equidistant to neutralize the centrifugal effect on the axis of the carrier and the radial force on the axis of the sun and the ring. These are two examples of strategies that are already applied at Eurocopter. Furthermore, it is also necessary to monitor epicyclical gears during their flight life, in order to ensure safety and also to improve maintenance. Its monitoring is therefore needed to be carried out with the most effective methods. Among Condition Monitoring Methods methods, vibration analysis using non-intrusive sensors works well with helicopter environment. Accelerometers are among the most suitable sensors for non-intrusive health monitoring of helicopters in terms of space, cost and qualification and have proved good performances for the monitoring of Eurocopter's helicopters.

Some analytical ([2] [3] [4] [5] ) and finite element models ([5] [6]) have been proposed to anticipate the

vibratory response. These predictions can be compared for a monitoring purpose to the vibratory response recorded on one accelerometer mounted on the ring. However, because of the various external forces applied to the system in flight, the complex mechanical design, multiple transfer paths, and the couplings between subsystems, it is quite difficult to predict precisely the vibratory response for condition monitoring. For this reason, the "signal oriented" model of vibrations for epicyclical gears is preferred for in-flight condition monitoring. According to some hypotheses, the suppression of some peaks and the amplification of some others have been demonstrated for equidistant planets. This model provides the pattern of vibrations under normal conditions. Consequently, it is possible to take advantage of this pattern for condition monitoring. In [7], McFadden and Smith introduce a signal-oriented model of vibrations to explain the characteristic patterns observed in equidistant eicyclical gears. Based on this model, McFadden designed in [8] a temporal algorithm for separating the synchronous average of the meshing of the planets. Forrester managed to patent this idea in [9]. Comparisons with embedded accelerometers can be found in [10]. This model and its consequences on the spectrum have been also studied for various geometric configurations [6].

The discovering of right indicators of epicyclical gears monitoring has been adressed in
[11] and [12]. In [11], the authors try several classic HUMS indicators and highlight that the decision is uncertain due to the variability of the indicators regarding the torque and the helicopter model considered. In [12], the authors apply the source separation method of [7] to create indicators based on the dispersion of amplitude and phase between consecutive planets. However, the robustness of the indicators for in fligth monitoring is weakened because the recording system and conditions for temporal separation method from [7] are too demanding for practical use.

In his PhD thesis [13], Patrick-Aldaco deals with the vibration-based model of [7] helicopter damage monitoring. For this reason, he creates a model-based diagnosis architecture studying the transverse crack on the carrier. Thanks to the finite-model, he finds a relation between the static shift angles on each planet and the crack length. The author also investigates the impact of non-zero static shift angles on the spectral patterns. This permits him to establish several indicators monitoring the evolution of the crack. However, its approach is purely spectral and he never establishes a theoretical link between the indicators and the crack length based on McFadden and Smith model.

The authors of [14] report an extensive and representative series of damage detection on one helicopter test bench including : bearing race damage and tooth cracks (sun, ring and planets). The authors successfully manage to detect all of these damages using classic HUMS indicators, but all of these methods need a reference value for applicability. Furthermore the authors do not study the issue of prognosis, the influence of the load of the aircraft or the unsteady conditions.

We have rewritten the vibration-based model in the spectral domain, and this formulation makes it easier to find the spectral influences of some mechanical defects, that is to say carrier's crack citing our example. Based on the structure of this model, we use the cyclostationary theory to introduce a damage indicator to monitor the global features of the epicyclical by checking that the spectral correlation produced by the suppressed peaks remains low. Then a source separation algorithm based on multi-sensor and cyclostationary analysis [15] is applied to estimate the "normal" and residual vibrations. These two methods are applied on a carrier's crack synthetised on a full scale test-bench.

# 2 Model of the measured vibration signal

## 2.1 Damaged-free model

### 2.1.1 Hypothesis for a healthy epicyclical gear

The vibration model rests on the following conditions: the signal is received on an accelerometer mounted radially or tangentially on the ring, $N$ planets mesh externally on the ring and the carrier is rotating at the frequency $\Omega$. In a normal operation, when no damage occurs, some additional hypotheses are introduced.

1. **The planets are equidistant**. The vibratory signal received from the $n^{th}$ planet is $(n-1)/(N\Omega)$ seconds late with respect to the $1^{rst}$ planet.
2. **The meshing vibrations are $1/(Z\Omega)$ periodic**. With $Z\Omega$ the meshing frequency of the epicyclical gear. Then the meshing vibrations $\gamma_n(t)$ for the $n^{th}$ planet can be decomposed on Fourier coefficients $A_m^n$.
3. **The transmission path between one planet and the accelerometer induces only amplitude modulation**. This modulation is noted $D_n(t)$.
4. **Meshing amplitude is independant of the planet**. The geometry, loads and transmission errors on each planet are the same. Consequently $A_m^n$ does not depend on $n$ and is noted $A_m$.
5. **The transmission path between one planet and the accelerometer is $\Omega$ periodic**.
6. **The planets have the same transmission paths**, but not all at the same time. Consequently the $D_n(t)$ are shifted versions of the same $D_1(t)$.

### 2.1.2 Temporal expression of the model

The signal received by the accelerometer is composed of the contribution of $N$ meshing planets. The following model is introduced.

$$v_n(t) = \underbrace{\gamma_n(t)}_{\text{hypothese 2}} \times \underbrace{D_n(t)}_{\text{hypothese 3}} \tag{1}$$

With:

$$\gamma_n(t) = \sum_{m=1..\infty} A_m \cos\left[2\pi m Z\Omega t + \Phi_m^n\right] \tag{2}$$

With $A_m$ and $\Phi_{n,m}$ the amplitude and the phase of the $m^{th}$ harmonic of the meshing from the $n^{th}$ planet. $A_m$ does not depend on $n$ because of hypothese 4. The hypothese 1 imposes that : $\Phi_m^n = \Phi_m^1 - 2\pi m Z(n-1)/N$.

According to hypothese 5 and 6, $D_n(t)$ can be decomposed in a temporal succession of $1/\Omega$ long windows $d(t)$ accounting for the modulation over one cycle and the shape of $d(t)$ does not depend on the planet considered. This repetition at frequency $\Omega$ is indexed by $k$.

$$D_n(t) = \sum_{k=-\infty..\infty} \underbrace{d\left(t - \frac{k}{\Omega} - \frac{n-1}{N\Omega}\right)}_{=d_n\left(t-\frac{k}{\Omega}\right)} = \left[\sum_{k\in\mathbb{Z}} \delta_{k/\Omega}(t)\right] * d\left(t - \frac{n-1}{N\Omega}\right) \tag{3}$$

### 2.1.3 Frequential expression of the model and properties of the signal

Since this problem is mainly periodic, the Fourier transform is applied to highlight the structure of the vibrations. With exponential notations, the meshing term becomes then for the $n^{th}$ planet:

$$\widehat{\gamma}_n(f) = \sum_{m=\mathbb{Z}-\{0\}} \frac{A_m}{2} e^{i\Phi_m^1} \exp\left(2\pi i \frac{mZ(n-1)}{N}\right) \times \delta_{mZ\Omega}(f) \tag{4}$$

With $A_{-m} = A_m$. And the modulation term for the $n^{th}$ planet is:

$$\widehat{D_n}(f) = \Omega\left[\sum_{k=-\infty..\infty} \delta_{k\Omega}(f)\right] \times \widehat{d}(f) \exp\left(2\pi i f \frac{n-1}{N\Omega}\right) \tag{5}$$

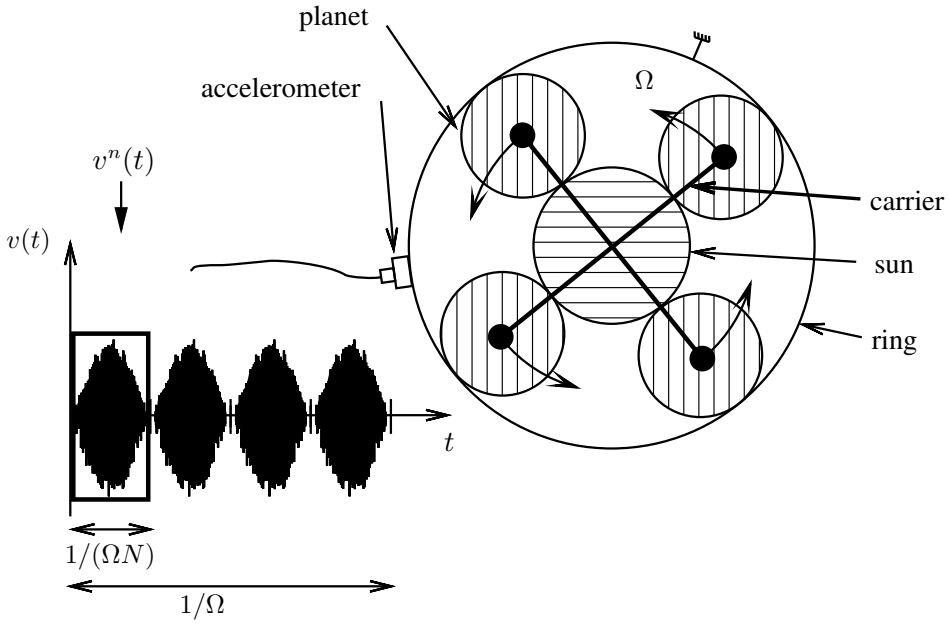


Figure 1: Diagram of an epicyclicar gear. An accelerometer mounted on its ring. In isotropic conditions, the accelerometer receives 4 uniformly distributed bell-shaped vibrations corresponding to the passing of the 4 planets.

The final signal containing all the contributions can be expressed in the Fourier domain. The modulating sidepeaks $k\Omega$ around the meshing frequency $mZ\Omega$ can then be expressed using classical properties on convolution of comb-filters:

$$\begin{aligned}\widehat{v}(f) &= \sum_{n=1}^{N} \widehat{v_n}(f) \\ &= \Omega \sum_{m=1..\infty} \frac{A_m}{2} e^{i\Phi_m^1} \sum_{k=-\infty..\infty} \widehat{d}(k\Omega) \times \underbrace{\sum_{n=1..N} \exp\left(2\pi i(n-1)\frac{k+mZ}{N}\right)}_{=C(m,k)} \delta_{(k+mZ)\Omega}(f)\end{aligned} \tag{6}$$

With $C(m,k) = N$ when $k + mZ$ is divisible by $N$ and 0 otherwise. Since $C(m,k) = C(m,k+N)$, then the spectrum shows local periodicity. In the following, the harmonics $(k+mZ)\Omega$ such that $C(m,k) = N$ are called the emerging harmonics and the other ones, the non-emerging harmonics. This pattern was previously discovered by [7]. The hypothesis detailed in section 2.1.1 implies that the signal has one spatial periodicity (rotation of $2\pi/N$), it is then natural to find that periodicity ($N\Omega$) in the spectrum when the speed is constant ($\Omega$).

### 2.1.4 Influence of the modulating window

The modulating window $d(t)$ accounts also for the transmission path between one planet and the accelerometer. It should be bell-shaped at the times corresponding to the less attenuated transfer paths. The first modulating window proposed by McFadden windows were rectangular and Hanning window, and more generally bell-shaped.

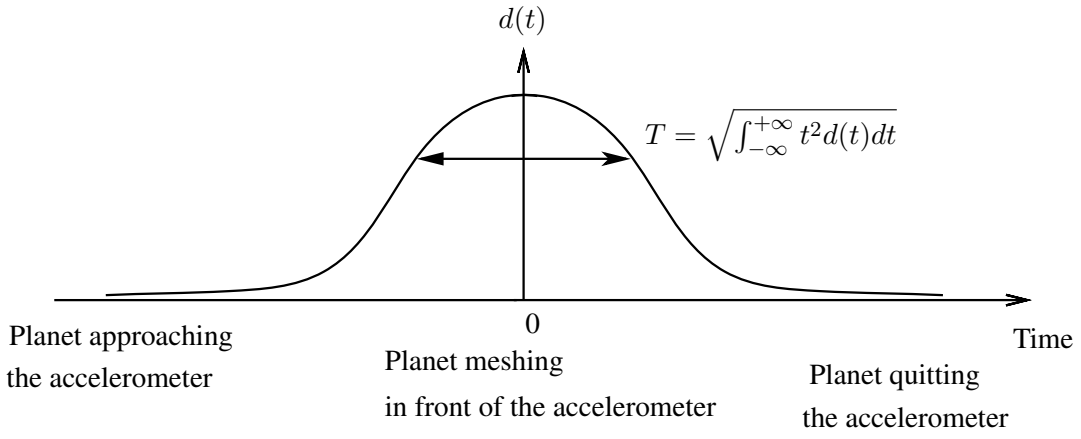


Figure 2: Shape of the centered modulating window with temporal dispersion $T$.

Let us note $T$, the temporal dispersion of the bell shape in $d(t)$ as described in figure 2, if one supposes that the only direct transfer path corresponds to the instant when the planet is meshing in front of the accelerometer (only one bell-shape). Then $\widehat{d}(f)$ is a band-pass filter in the Fourier domain of bandwidth $1/T$. Since the mechanical properties of system impact the transfer path, then it impacts the shape of $d(t)$ and $\widehat{d}(f)$ and consequently the amount of observable $1\Omega$ side peaks in equation 6 around the harmonics of the meshing frequency $Z\Omega$. In practice $1/T \approx \Omega/(2N)$, and consequently for $|k| < N/2$ the harmonics are visible. Moreover, the influence of the smoothness of the window has been investigated and it appears also that the amount non-zeros side-peaks decrease with the regularity at one fixed time duration $T$. Consequently under normal conditions a decrease in the amount of observable side-peaks means that the time duration or regularity could increase.

## 2.2 Modelisation of a transverse carrier crack

When a transverse crack breaks out on the carrier, the geometrical position of the planets change, and the angular distance between adjacent planets are shifted. The temporal shift induced by the crack is $\epsilon/\Omega$. For this reason, the following hypothesis are introduced:

- The crack only influences the position of one planet (by convention the first planet $n = 1$). The author of [13] gives a quantitative discussion about this issue. Further calculations can be derived by multiple phase shifts, however the main conclusions remain the same.
- The crack does not influence the load distribution between the planets. The hypothesis is strong, since the high level of hyperstaticity and the impact of a damage is likely to change the load sharing between the planets during the functionning.
- $\epsilon$ can be decomposed into a *static* component $\epsilon_0$ (constant during the recording time), a *"breathing"* component $\epsilon_1 \times \sin(\Omega t + \phi)$ accounting for the opening-closing with phase reference $\phi$ ([16]) phenomenon and a *random* component independant and identically distributed $\epsilon_2$ accounting for the unsteady load variations.

## 2.3 Consequence of a transverse carrier crack

It is then possible to derive the influence of a crack on the model 1. This crack should perturbates the modulating window and also the meshing part. However, the amplitude of these perturbations have not the

same order of magnitude for the two terms. Let us note $\gamma_1(t,\epsilon)$ and $d_1(t,\epsilon)$ the meshing vibrations and modulating window of the $1^{rst}$ planet with a phase shift $\epsilon$. The quantitative influence of small values of $\epsilon$ are now studied. The symbol $\|\|_t$ denotes the averaged quadratic norm over the time $t$:

$$\begin{aligned}
\|\gamma_1(t,\epsilon)-\gamma_1(t,\epsilon=0)\|_t &\approx \epsilon \left\| \frac{\partial \gamma_1(t,\epsilon)}{\partial \epsilon} \right\|_t \\
&= \left\| \sum_{m=1..\infty} A_m(\cos\left[2\pi m Z\Omega(t+\epsilon/\Omega)+\Phi_m^1\right]-\cos\left[2\pi m Z\Omega t+\Phi_m^1\right]) \right\|_t \\
&\approx \left\| \sum_{m=1..\infty} A_m 2\pi m Z\epsilon \sin\left[2\pi m Z\Omega t+\Phi_m^1\right] \right\|_t \\
&\geq 2\pi Z\epsilon \left\| \sum_{m=1..\infty} A_m \sin\left[2\pi m Z\Omega t+\Phi_m^1\right] \right\|_t \\
&\geq 2\pi Z\epsilon \|\gamma_1(t,\epsilon=0)\|_t
\end{aligned} \tag{7}$$

And for the modulating window:

$$\|d_1(t,\epsilon)-d_1(t,0)\|_t \approx \epsilon \left\| \frac{\partial d_1(t,\epsilon)}{\partial \epsilon} \right\|_t \tag{8}$$

[6] approximates the window by a Hann function: $d_1(t)=\mathbb{1}_{[-T/2;T/2]}\cos(\pi t/T)^2$, with this model one can calculate the derivative:

$$\|d_1(t,\epsilon)-d_1(t,0)\|_t \approx \pi\epsilon/(T\Omega)\left\|\mathbb{1}_{[-T/2;T/2]}\sin(2\pi t/T)\right\|_t = \pi\epsilon/T\,\|d_1(t,0)\|_t \tag{9}$$

Moreover, since $2\pi Z\epsilon/(\pi\epsilon/(T\Omega)) \approx 2\times Z/N \approx 2\times 130/8 \approx 30$, then the influence of the crack on the modulating window is approximately 30 times smaller than on the meshing vibrations. Consequently, the modulating window is considered in the following unaffected for first order approximation. Then only the influence on the meshing vibrations is considered. The meshing part $\widehat{\gamma_1}$ of the vibrations in the first planet is now written with its exponential form to allow easy manipulation of the phase shift.

$$\begin{aligned}
\widehat{\gamma_1}(f) &= \sum_{m\in\mathbb{Z}-\{0\}} A_m/2\exp\left[2\pi i m Z\Omega\left(t-\frac{\epsilon}{\Omega}\right)+i\Phi_m^0\right] \\
&= \sum_m A_m/2\exp\left[2\pi i m Z\left(\Omega t-\epsilon_0-\epsilon_1\cos(\Omega t+\phi)-\epsilon_2(t)\right)+i\Phi_m^0\right] \\
&= \sum_m A_m/2\exp\left[-2\pi i m Z\epsilon_0+i\Phi_m^0\right] \\
&\quad\times\exp\left[2\pi i m Z\left(\Omega t-\epsilon_1\cos(\Omega t+\phi)\right)\right] \\
&\quad\times\exp\left[-2\pi i m Z\epsilon_2(t)\right]
\end{aligned} \tag{10}$$

However, it is possible to decompose $\exp\left[2\pi i m Z\left(\Omega t-\epsilon_1\cos(\Omega t+\phi)\right)\right]$ using Bessel functions (frequency modulation):

$$\begin{aligned}
\gamma_1(t) = &\sum_{m\in\mathbb{Z}-\{0\}} A_m/2\exp\left[-2\pi i m Z\epsilon_0+i\Phi_m^0\right] \\
&\times\left\{\sum_{q\in\mathbb{Z}} J_q(-2\pi i m Z\epsilon_1)\times\exp\left(2\pi i(mZ+q)\Omega t+q\phi\right)\right\}\times\exp\left[-2\pi m Z\epsilon_2(t)\right]
\end{aligned} \tag{11}$$

Let us note $E_m(f)$ the Fourier transformation of $\exp(-2i\pi mZ\epsilon_2(t))$. Then taking the Fourier transformation of equation 11:

$$\widehat{\gamma_1}(f) = \sum_{m\in\mathbb{Z}-\{0\}} \frac{A_m}{2} \exp\left[-2\pi imZ\epsilon_0 + i\Phi_m^0\right] \times \left\{ \sum_{q\in\mathbb{Z}} J_q(-2\pi imZ\epsilon_1) \times \delta_{(mZ+q)\Omega} \times e^{iq\phi} \right\} * E_m(f) \tag{12}$$

Then the final contribution of the first planet is calculated in the Fourier domain with the modulating window $d_1$:

$$\begin{aligned}\widehat{\gamma_1 d_1} = \widehat{\gamma_1} * \widehat{d_1} = &\sum_{m\in\mathbb{Z}-\{0\}} \frac{A_m}{2} \exp\left[-2\pi imZ\epsilon_0 + i\Phi_m^0\right] \times \\ &E_m * \left\{ \sum_{q\in\mathbb{Z}} J_q(-2\pi imZ\epsilon_1) e^{iq\phi} \times \delta_{(mZ+q)\Omega} \right\} \\ &* \left\{ \Omega \left[ \sum_{k\in\mathbb{Z}} \widehat{d_1}(k\Omega) \times e^{-2\pi i \frac{kn}{N}} \delta_{k\Omega} \right] \right\}\end{aligned} \tag{13}$$

$$\begin{aligned}=&\Omega \sum_{m\in\mathbb{Z}-\{0\}} \frac{A_m}{2} \exp\left[-2\pi imZ\epsilon_0 + i\Phi_m^0\right] \times E_m * \\ &\left\{ \sum_{q,k\in\mathbb{Z}} J_q(-2\pi imZ\epsilon_1) e^{iq\phi} \widehat{d_1}(k\Omega) \times e^{-2\pi i \frac{kn}{N}} \delta_{(mZ+q+k)\Omega} \right\}\end{aligned} \tag{14}$$

With the variable change $a = q + k$ and $b = q$:

$$\begin{aligned}\widehat{\gamma_1} * \widehat{d_1} =&\Omega \sum_{m\in\mathbb{Z}-\{0\}} \frac{A_m}{2} \exp\left[-2\pi imZ\epsilon_0 + i\Phi_m^0\right] \times E_m \\ &* \left\{ \sum_{a,b\in\mathbb{Z}} J_b(-2\pi imZ\epsilon_1) e^{ib\phi} \widehat{d_1}((a-b)\Omega) \times e^{-2\pi i \frac{(a-b)n}{N}} \delta_{(mZ+a)\Omega} \right\}\end{aligned} \tag{15}$$

Since $E_m$ and $\delta_{(mZ+a)\Omega}$ are the only non-constant terms, they are gathered:

$$\begin{aligned}\widehat{\gamma_1} * \widehat{d_1} =&\Omega \sum_{m\in\mathbb{Z}-\{0\}} \frac{A_m}{2} \exp\left[-2\pi imZ\epsilon_0 + i\Phi_m^0\right] \\ &\times \left\{ \sum_{a,b\in\mathbb{Z}} J_b(-2\pi imZ\epsilon_1) e^{ib\phi} \widehat{d_1}((a-b)\Omega) \times e^{-2\pi i \frac{(a-b)n}{N}} \right. \\ &\left. E_m * \delta_{(mZ+a)\Omega} \right\}\end{aligned} \tag{16}$$

This formula can be written in a more compact form where $m$ is the index of the meshing harmonics and $a$ is the index of the $1\Omega$ modulations. The term inside the brace denotes the amplitude change because of the crack.

$$\begin{aligned}\widehat{\gamma_1 d_1}(f) =&\Omega \sum_{m,a} \frac{A_m}{2} \times e^{i\Phi_m^0} \\ \textit{static opening } \rightarrow \quad &\times e^{-2\pi imZ\epsilon_0} \\ \textit{breathing and modulating window } \rightarrow \quad &\times \left\{ \sum_b J_b(-2\pi imZ\epsilon_1) e^{ib\phi} \widehat{d_1}\left((a-b)\,\Omega\right) e^{-2\pi i \frac{(a-b)n}{N}} \right\} \\ \textit{random load } \rightarrow \quad &\times E_m(f - (mZ+a)\Omega)\end{aligned} \tag{17}$$

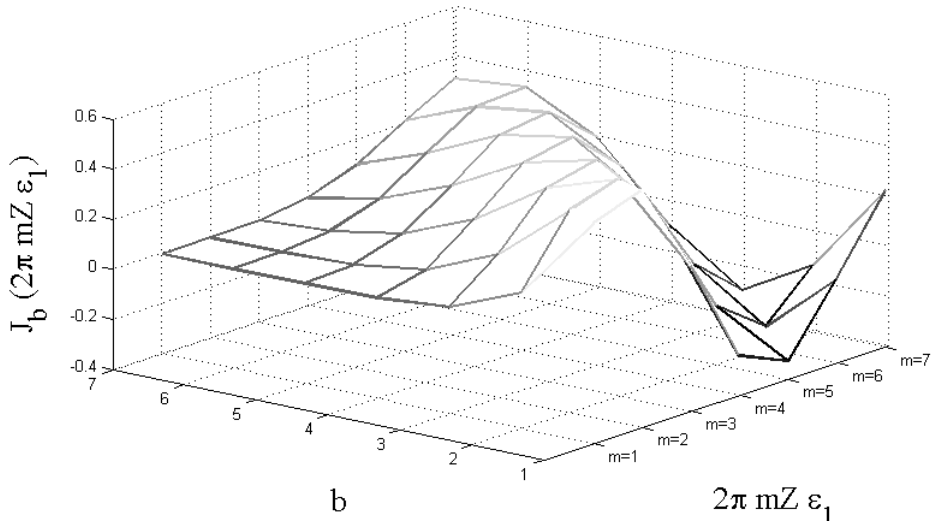


Figure 3: Evolution of the $J_b$ bessel function of first kind with respect to $(2\pi mZ\epsilon_1)$ and $b$. The number of teeth of the ring is 130 and the breathing amplitude $\epsilon_1$ is half-minute of arc.

It is then possible to explain the quantitative influence of the three components of the crack on the distribution of $1\Omega$ modulations around the meshing harmonics. These $1\Omega$ modulations are the harmonics separated of the meshing harmonics by a multiple of $1\Omega$.

- *static opening* : $\epsilon_0$ creates additional $1\Omega$ modulations around the meshing frequency $Z\Omega$. The frequential dispersion is given by $d$ and is $\approx 1/T \approx \Omega/N$.
- *breathing phenomenon* : if $\epsilon_1 = 0$, then $b = 0$ and there would not be any $1\Omega$ modulations in the basis attached to the carrier and the accelerometer would receive $1\Omega$ modulation from only the static opening. Let us suppose that the breathing phenomenon produces a fluctuation of half-minute of arc: $\epsilon_1 = 0.5/360$ with $Z = 130$ teeth on the ring. The figure 3 shows the amplitude of the $b^{th}$ modulation at $1\Omega$ since the breathing around the $m^{th}$ meshing. For small values of $b$, the amplitude of the Bessel function is almost-periodic with respect to $m$, and then the position of the first zero-crossing amplitude ($m = 3$ in figure 3) changes rapidly with $\epsilon_1$. Moreover if $\pi mZ\epsilon_1 >> 1$, then the amplitude decreases due to the Bessel function does not depend on $b$ and is slow. Consequently the breathing phenomenon creates strong and complex modulations in the spectrum with numerous $1\Omega$ modulations around meshing harmonics.
- *random load distribution* : the term $\epsilon_2$ transforms $\delta_{(mZ+a)\Omega}(f)$ into $E_m(f - (mZ + a)\Omega)$. Then $\epsilon_2$ contributes to the randomization of the amplitudes, moreover as these amplitudes are randomized by the same factor $E_m$, they will be then statistically correlated.

On the one hand, the combination of the static deformation and of the breathing phenomenon contributes to create $1\Omega$ modulations around the harmonics of the meshing, and on the other hand the random deformation creates statistical links between these harmonics. Consequently, if a transverse crack follows the hypothesis defined before, then the Fourier transform will show spectral correlations at frequency $1\Omega$. Spectral correlation between harmonics can be reformulated in the cyclostationary theory developped by [17]. It is then possible to use the tools provided by the study of cyclostationary.

## 2.4 Indicators

### 2.4.1 Cyclostationary coherence

Since the meshing vibrations following the hypotheses of 2.1.1 can be seen as cyclostationary processes (paragraph 2.2), it is possible to use the tools measuring the spectral dependance between the harmonics of interest in the signal. The cyclic coherence permits to mesure the correlation between two harmonics located at $f - \alpha/2$ and $f + \alpha/2$, with $f$ the frequency and $\alpha$ the cyclic frequency. In [15], the cyclic coherence is introduced with:

$$\lambda_{YX}(f;\alpha) = \frac{E\left\{dY\left(f\right)dX^{*}\left(f+\alpha\right)\right\}}{\left[E\left\{\left|dY\left(f\right)\right|^{2}\right\}E\left\{\left|dX\left(f+\alpha\right)\right|^{2}\right\}\right]^{1/2}} \in [-1;1] \tag{18}$$

Where $dY$ is called the spectral increment of the signal $y(t)$ according in Cramer's decomposition. The cyclic coherence can be seen as an extension of the power spectral density to the second order and is pratically estimated with the Welch estimator, [15].

The design of new indicators can rest on the combination of this tool with the knowledge of the spectral patterns relating to the epicyclic gear with or without cracks. It can be used for assessing the correlation between two known harmonics in the spectrum and especially two symetric $1\Omega$ modulations around the meshing harmonics. Since the model of equation 17 deduced from a transverse crack shows correlations between the $1\Omega$ modulations around the harmonics of the meshing frequency $Z\Omega$, the frequency $f$ in equation 18 is set to multiples of $Z\Omega$ and the frequency $\alpha$ is set to multiples of $\Omega$. Based on this conclusion, it is proposed to use $|\lambda_{YX}(Z\Omega;2\Omega)|$ to check the spectral correlation between the right $1\Omega$ sidepeak and the left $1\Omega$ sidepeak around the fundamental of the meshing frequency $Z\Omega$. It is then an indicator for checking the distance between the state of the current system and cracked-like system.

### 2.4.2 Blind component separation

The cyclostationary structure of the signal can also lead to "denoising" algorithms. In our situation, rather than searching for signals related to physical sources (e.g. the planets), [18] suggests to search for signals related to a physical phenomenon that is not necessarily spacially defined (e.g. the meshing of all the planets). The two components of interest are here, the "normal" meshing vibrations and the meshing vibrations with a crack. The conclusion of the section 2.2 proves that these two components are respectively related to $N\Omega$ and $1\Omega$ modulations around the meshing harmonics $mZ\Omega$ ($m \in \mathbb{N}^{*}$). The algorithm selected for finding these two components is described in [19] and is made of two (SUBPLEX and MCR) techniques taking advantage of the statistical independence of the source of interest regarding the "noise" (SUBPLEX) and the statistical periodicity of that vibrating source (SUBPLEX and MCR). This algorithm has been selected as all the cyclic frequencies of interest are used simultaneously and the relative error of reconstruction decreases linearly with the length of the inputs. This algorithm requires to set a weigthening matrix that can be chosen to minimize its variance of the solution under the asumption that the source of interest does not contain first order cyclostationary features. This asumption cannot be verified for the epicyclical gear around the meshing frequencies, see equation 6. This weigthening matrix has then been changed to a diagonal matric around the harmonics of the meshing frequency.

In addition to the extracted components, this algorithm produces a decomposition matrix at each frequency $f$ to find the components of interest in the spectrum. Moreover, it is possible to extract an eigenvalue $\rho(f)$ showing how much component of interest is present in all signals at frequency $f$. $\rho(f)$ indicates the frequency bands where the signal-to-noise ratio is the best. Let us note $\rho_{\text{normal}}(f)$ and $\rho_{\text{crack}}(f)$ the eigenvalues for the extraction of normal vibrations and for the extraction of vibrations with a crack. Consequently, the ratio $\rho_{\text{crack}}(f)/\rho_{\text{normal}}(f)$ indicates the ratio between the component related to a cracked system and the

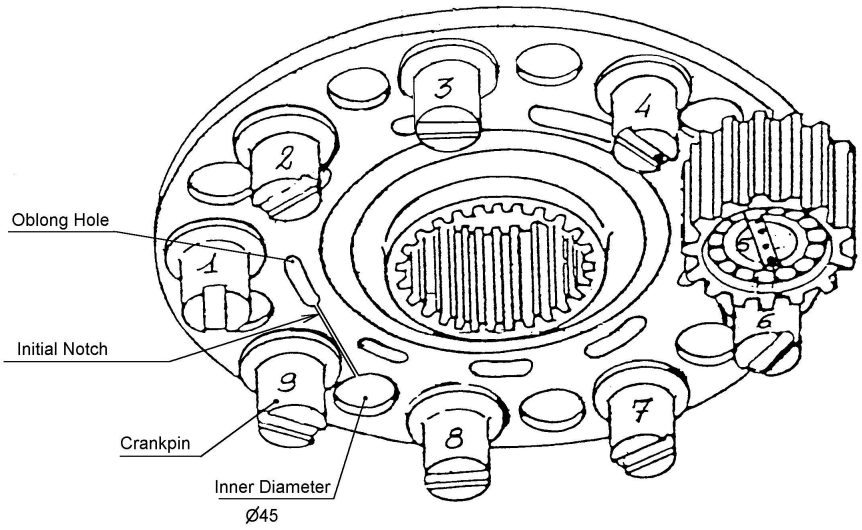


Figure 4: Second stage of an Super-Puma epicyclical gear with a crack on the carrier.

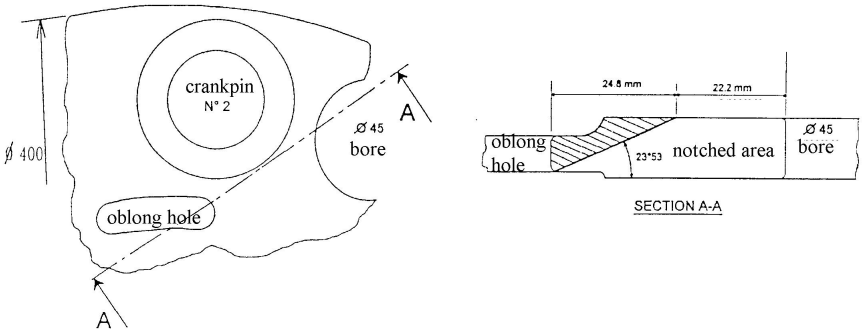


Figure 5: Description of the crack on the carrier presented in figure 4.

component related to a normal system at the frequency $f$ for all the accelerometers available. Moreover, the section 2 shows that the signal is expected to show $N\Omega$ modulation around the meshing frequency under normal vibrations and $1\Omega$ spectral correlation around the harmonics of the meshing frequency $Z\Omega$ with a crack on the carrier. Then the indicator $\rho_{\text{crack}}(Z\Omega)/\rho_{\text{normal}}(Z\Omega)$ shows the ratio of cracked-carrier vibrations over normal vibrations at the fundamental of the meshing frequency. This frequency $Z\Omega$ has been chosen because as it is the fundamental, it carries most of the energy and the global shape of the vibrations.

# 3 Applications on test bench data

## 3.1 Description of the experiment

### 3.1.1 Presentation of the test bench

During the 90's, the CAA (the UK Civil Aviation Authority) made funds available for a rig test programme performed by Eurocopter to promote research on Helicopter Health Monitoring. This project permitted the testing a Super-Puma epicyclical gear. This system contains $N = 9$ satellites and $Z = 130$ teeth on the ring. The initial defect was designed to allow for crack initiation and propagation under the vibratory loads. A notch was seeded into the web of the upper stage planet carrier in order to trigger the crack.

Figure 6: View from below (rigth) and above (left) the carrier.

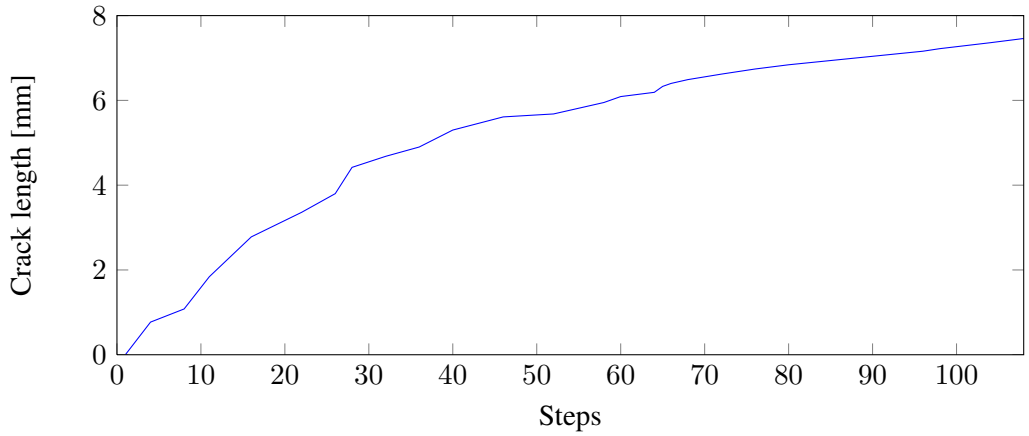


Figure 7: Crack growth in terms of cycles.

### 3.1.2 Methodology and measurements

The crack is initiated by deliberately reducing its fatigue strength at the correct location, because it allows proper control of the crack location and the collection of data in test conditions close to normal operation. The specified dimensions of the notch were thus based on the fractographic analysis of the cracked component. The notch was specified so as to simulate the crack when it was supposed to start to propagate under the vibratory loads. The specified notch location and dimensions are given in figures 4 and 5. Pictures of the final crack are shown in figure 6. One of the major difficulties is to locate, size and orientate the notch so as to allow the initiation of the expected crack under normal loads. The defect therefore has to be large enough to create the stress concentration which will lead to the crack initiation. However, the data generated has to be used to assess the effectiveness of the vibration analysis techniques. The defect therefore has to be small enough to allow the crack to propagate under the test loads for as long as possible. The finding of a compromise was achieved using finite elements codes and crack propagation models. The crack was initiated from multiple start points at the notch bottom and propagated under vibratory loads, approximately in the plane of the notch. The crack growth is depicted in the figure 7. The component was tested for 108 steps. During one step the input torque is 960kW (close to the twin engine maximum continuous power) during 15 minutes and 768kW during 5 minutes. Recordings of 1 second are available for the cycles 1, 21, 43, 65, 86 and 108. The frequency bandwidth is 12 kHz, the measuring range is 500g, the recording length is 1 second and the speed of the rotor is $\Omega = 6.15$Hz.

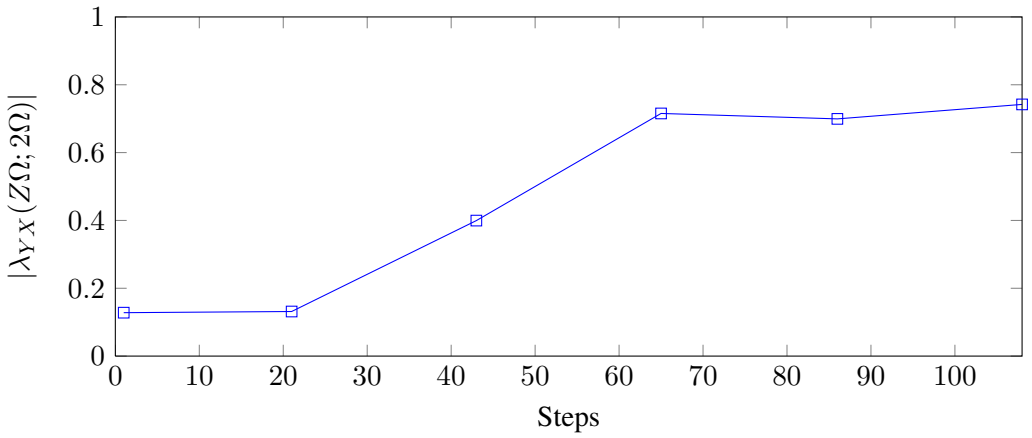


Figure 8: Eigenvalues from the $|\lambda_{YX}(Z\Omega;2\Omega)|$ ($\in [0;1]$) in terms of cycles.

## 3.2 Results of the indicators

### 3.2.1 Cyclic coherence

The cyclic coherence $|\lambda_{YX}(Z\Omega;2\Omega)|$ defined before is applied and the results are displayed in figure 8. The indicator permits to follow the growth of the crack. The indicator stays noticeably quite small ($< 0.20$) when the crack starts increasing. Then the indicator grows linearly when the cracks increases, until it reachs an asymptote. It is enforced that the consequence of the crack on the phase shift comes from its whole geometry and not only its lentgh, and so one cannot establish a one-to-one relationship between the two curves. However the global shapes of the curves in figures 7 and 8 are in accordance and the infuence of the crack growth is quantitatively observable with the proposed indicator.

### 3.2.2 Blind component separation

The algorithm and the indicator described in 2.4.2 are applied to extract and measure the normal and damaged meshing vibrations. The normal vibrations and damaged vibrations are displayed in figure 10 for step 1. The y-units have been changed for intellectual property issues. The passing of the $N = 9$ planets in one cycle (denoted by black vertical lines) is visible in the normal vibrations. Moreover, the temporal dispersion $T$ of the modulating window $d(t)$ appears to be about $T \approx 1/(\Omega N)$, which confirms the asumption of section 2.1.4. The eigenvalues $\rho_{\text{crack}}(f)$ and $\rho_{\text{normal}}(f)$ are displayed in figure 9 around the fundamental of the meshing frequency. It appears that the content of abnormal vibrations in this frequency band is much higher for the last recording rather than for the first recording. This tendancy is inverted for the normal vibrations. This shows the relevance of these indicators for detecting a transverse carrier crack. The indicator $\rho_{\text{crack}}(Z\Omega)/\rho_{\text{normal}}(Z\Omega)$ is displayed in figure 11 in Decibel units. Like the cyclic coherence, it permits to follow the growth of the crack. There is a drop at step 21, that may due to the small recording time that lowered the frequency resolution and then the accuracy of the indicator. The indicator crosses 0 Decibel after the step 68, it means that after the $68^{th}$ step the abnormal vibrations are prevailing at the fundamental of the meshing frequency. This indicator permits to measure the influence of the damaged vibrations against the normal vibrations.

# 4 Conclusion

In this paper, the problem of transverse crack in epicyclical gears has been adressed. For that purpose a theoretical vibrations-based model has been introduced. This model describes the patterns in the vibration

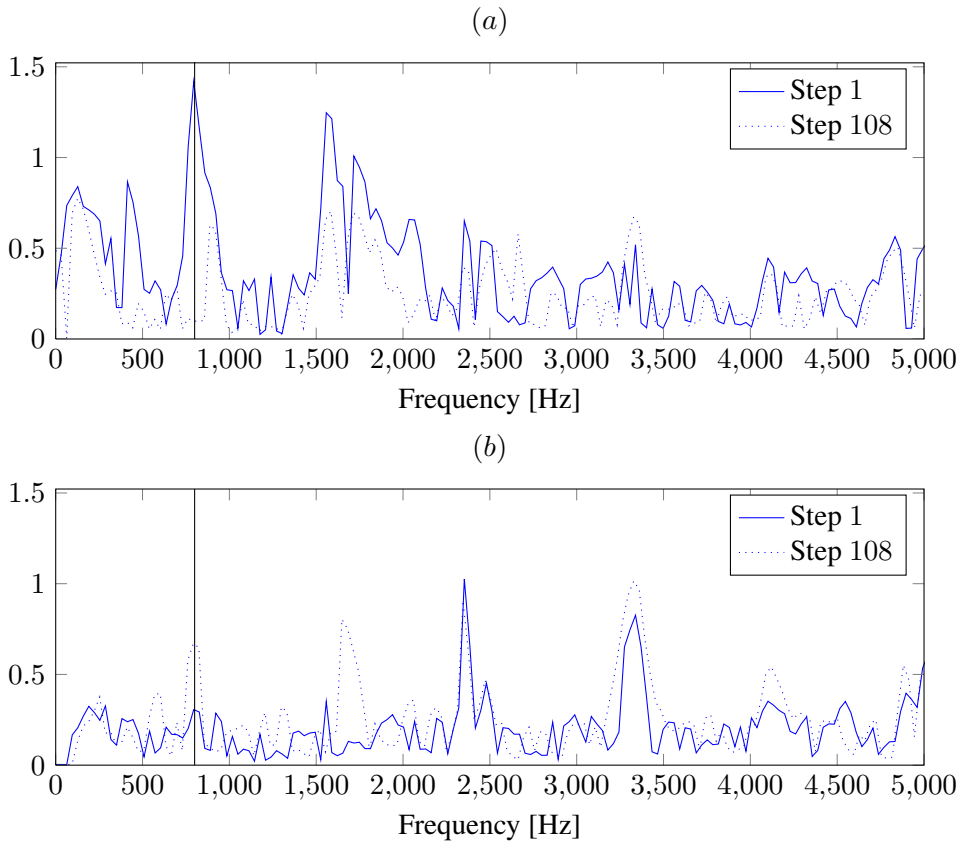


Figure 9: Eigenvalues from the blind component separation in terms of cycles. The top graph shows the $\rho_{\text{normal}}(f)$ ($(a)$) and the bottom one the damaged vibrations $\rho_{\text{crack}}(f)$, $(b)$. The vertical lines point to the fundamental of the meshing frequency $Z\Omega = 800$ Hz.

spectrum in a damage-free case and with a phase shift on one planet. The phase shift has been modelled with a static component, a "breathing" component and a random component. The spectrum resulting from a phase shift shows spectral correlation at the frequency of the rotor and around the meshing frequencies. Two indicators that exploit spectral correlation are then proposed to assess the presence of such a damage. These indicators are then tested on data recorded on a Eurocoper test bench. The experiment of the test bench consist of an artificially seeded carrier's crack fifteen years ago. The two indicators manage to follow the increase of the crack. This article shows the effectiveness of the latest methods of signal processing for epicyclical gears monitoring on a dataset with old recording conditions. New experiments will be carried out by Eurocopter with state-of-the-art recording systems for monitoring smaller and more complex damages affecting the components of the epicyclic gear. The proposed methods, that have been successfully applied in this paper, will be then applied in the next experiments.

The authors would like to thank the CAA (Dave Howson) and the Eurocopter team who performed and supervised the experimental tests.

## References

[1] Henriot. *Engrenages , Conception, fabrication, mise en oeuvre*. Usine Nouvelle, 2007.

[2] R.G. Parker and X. Wu. Vibration modes of planetary gears with unequally spaced planets and an elastic ring gear. *Journal of Sound Vibration*, 329:2265–2275, May 2010.

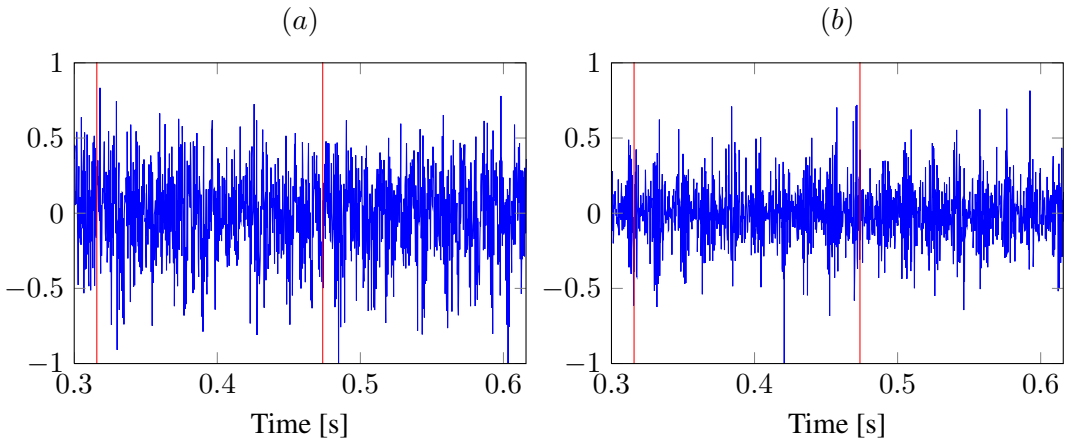


Figure 10: Raw vibrations $(a)$ and extracted normal vibrations $(b)$ at the first step between 0.28 s and 0.57 s. The vertical lines denote the top rotor and permit to see the $N = 9$ planets. Vertical units have been changed.

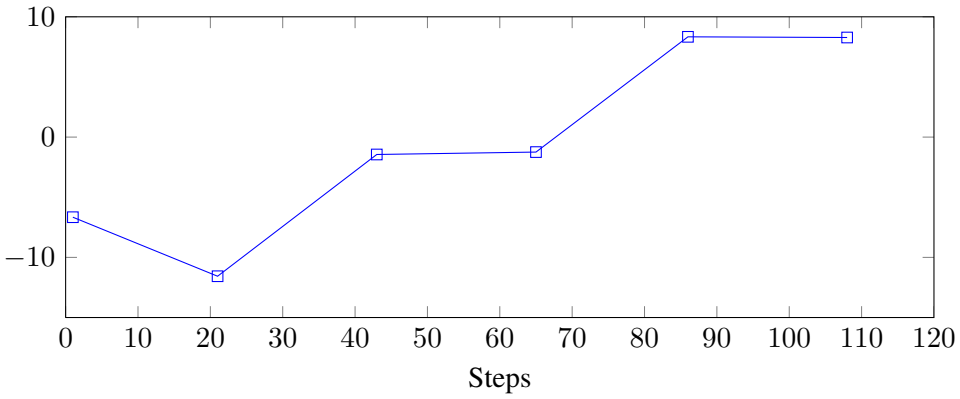


Figure 11: Indicator $\rho_{\text{crack}}(Z\Omega)/\rho_{\text{normal}}(Z\Omega)$ in terms of cycles. The ratio is expressed in Decidel.

[3] ROBERT G. Parker. A physical explanation for the effectiveness of planet phasing to suppress planetary gear vibration. *Journal of Sound and Vibration*, 236(4):561 – 573, 2000.

[4] Woohyung Kim, Ji Yeong Lee, and Jintai Chung. Dynamic analysis for a planetary gear with time-varying pressure angles and contact ratios. *Journal of Sound and Vibration*, 331(4):883–901, 2012.

[5] V. Abousleiman and P. Velex. A hybrid 3d finite element lumped parameter model for quasi static and dynamic analyses of planetary epicyclic gear sets. *Mechanism and Machine Theory*, 41(6):725 – 748, 2006.

[6] Inalpolat. *a theoretical and experimental investigation of modulation sidebands of planetary gear sets*. PhD thesis, Ohio State University, Mechanical Engineering, 2009.

[7] P.D. McFadden and J.D. Smith. An explanation for the asymmetry of the modulation sidebands about the tooth meshing frequency in epicyclic gear vibration. *Proceedings of the Institution of Mechanical Engineers*, 199:65–70, 1985.

[8] P. D. McFadden. A technique for calculating the time domain averages of the vibration of the individual planet gears and the sun gear in an epicyclic gearbox. *Journal of Sound and Vibration*, 144(1):163 – 172, 1991.

[9] Forrester. Method for the separation of epicyclic planet gear vibration signatures, 2001.

[10] Marc Ryan De Smidt. Internal vibration monitoring of a planetary gearbox. Master's thesis, University of Pretoria Mechanical and Aeronautical Engineering, 2010.

[11] J. Keller and P. Grabill. Vibration monitoring of a uh-60a main transmission planetary carrier fault. In *the American Helicopter Society 59th Annual Forum*, Phoenix, Arizona, May 2003.

[12] David M. Blunt and Jonathan A. Keller. Detection of a fatigue crack in a uh-60a planet gear carrier using vibration analysis. *Mechanical Systems and Signal Processing*, 20(8):2095 – 2111, 2006.

[13] Romano Patrick-Aldaco. *A Model Based Framework for Fault Diagnosis and Prognosis of Dynamical Systems with an Application to Helicopter Transmissions*. PhD thesis, Georgia Institute of Technology, Atlanta, GA, 2007.

[14] Ryan Ehinger, Jason Fetty, Kelsen LaBerge, and David Lewicki. Planetary gearbox fault detection using vibration separation techniques. In *AHS*, 2011.

[15] Jérôme Antoni. Cyclic spectral analysis in practice. *Mechanical Systems and Signal Processing*, 21(2):597 – 630, 2007.

[16] IM Mayes and WGR Davies. The vibrational behaviour of a rotating shaft system containing a transverse crack. In *IMechE Conf. Vibration in Rotating Machinery*, 1976.

[17] W.A. Gardner and C.M. Spooner. The cumulant theory of cyclostationary time-series. i. foundation. *Signal Processing, IEEE Transactions on*, 42(12):3387 –3408, dec 1994.

[18] Jérôme Antoni and Simon Braun. Editorial. *Mechanical Systems and Signal Processing*, 19(6):1163 – 1165, 2005. Blind Source Separation.

[19] Roger Boustany and Jérôme Antoni. Blind extraction of a cyclostationary signal using reduced-rank cyclic regression–a unifying approach. *Mechanical Systems and Signal Processing*, 22(3):520 – 541, 2008.